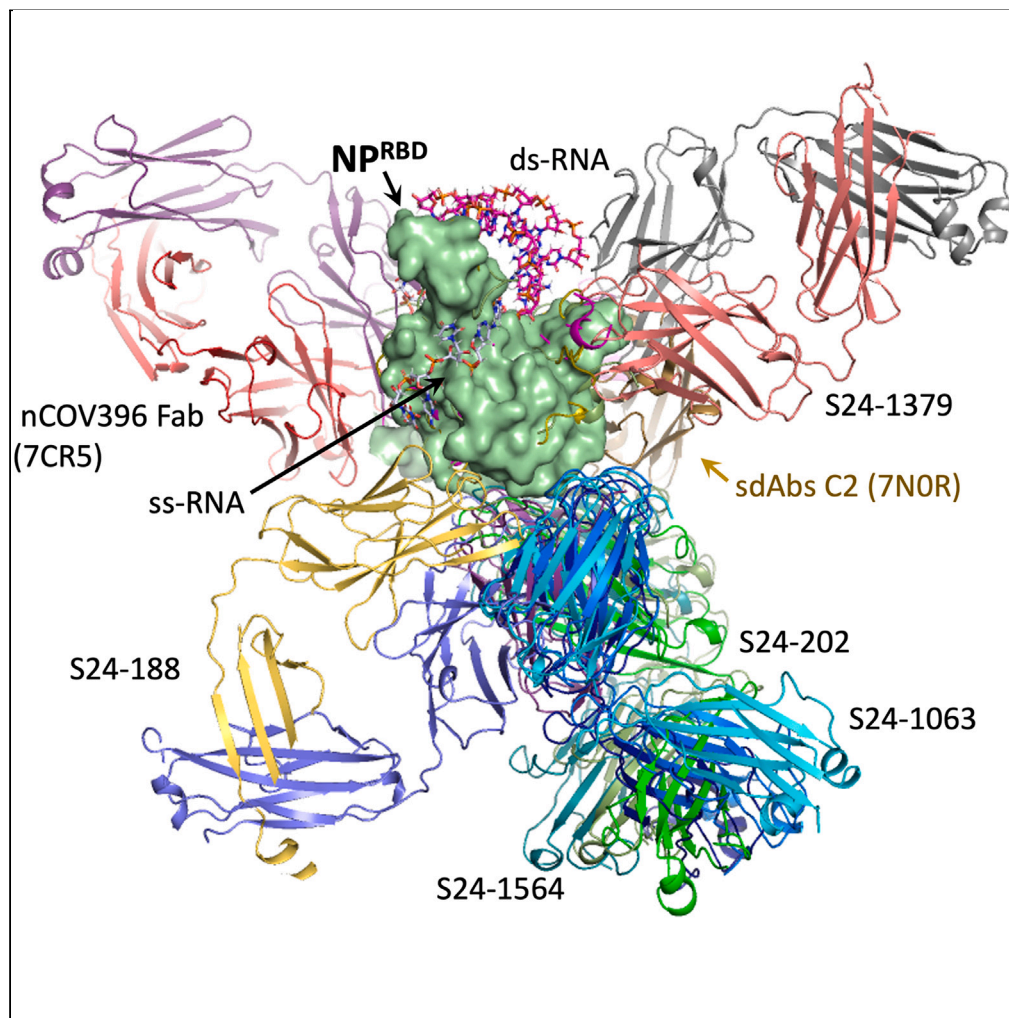


## Article

## Epitopes recognition of SARS-CoV-2 nucleocapsid RNA binding domain by human monoclonal antibodies



Youngchang Kim,  
Natalia Maltseva,  
Christine Tesar, ...,  
Patrick Wilson,  
Karolina  
Michalska, Andrzej  
Joachimski

andrzej@anl.gov

**Highlights**

Structures of SARS-CoV-2 nucleocapsid RNA-binding domain, NP<sup>RBD</sup>, show key epitopes

The mAbs-NP<sup>RBD</sup> complexes reveal distinct CDRs recognizing divergent epitopes

The models of nucleocapsid dimer and the RNA complexes reveal key mutations

Simulations show how antibody disrupts the natural dynamic fluctuation of nucleocapsid

Kim et al., iScience 27, 108976  
February 16, 2024 © 2024 The  
Authors.  
[https://doi.org/10.1016/  
j.isci.2024.108976](https://doi.org/10.1016/j.isci.2024.108976)

## Article

## Epitopes recognition of SARS-CoV-2 nucleocapsid RNA binding domain by human monoclonal antibodies

Youngchang Kim,<sup>1,2</sup> Natalia Maltseva,<sup>1,2</sup> Christine Tesar,<sup>1,2</sup> Robert Jedrzejczak,<sup>1,2</sup> Michael Endres,<sup>1,2</sup> Heng Ma,<sup>3</sup> Haley L. Dugan,<sup>4</sup> Christopher T. Stamper,<sup>4</sup> Changsoo Chang,<sup>1,2</sup> Lei Li,<sup>4</sup> Siriruk Changrob,<sup>4</sup> Nai-Ying Zheng,<sup>4</sup> Min Huang,<sup>4</sup> Arvind Ramanathan,<sup>3</sup> Patrick Wilson,<sup>5</sup> Karolina Michalska,<sup>1,2</sup> and Andrzej Joachimiak<sup>1,2,4,6,\*</sup>

## SUMMARY

**Coronavirus nucleocapsid protein (NP) of SARS-CoV-2 plays a central role in many functions important for virus proliferation including packaging and protecting genomic RNA. The protein shares sequence, structure, and architecture with nucleocapsid proteins from betacoronaviruses. The N-terminal domain (NP<sup>RBD</sup>) binds RNA and the C-terminal domain is responsible for dimerization. After infection, NP is highly expressed and triggers robust host immune response. The anti-NP antibodies are not protective and not neutralizing but can effectively detect viral proliferation soon after infection. Two structures of SARS-CoV-2 NP<sup>RBD</sup> were determined providing a continuous model from residue 48 to 173, including RNA binding region and key epitopes. Five structures of NP<sup>RBD</sup> complexes with human mAbs were isolated using an antigen-bait sorting. Complexes revealed a distinct complement-determining regions and unique sets of epitope recognition. This may assist in the early detection of pathogens and designing peptide-based vaccines. Mutations that significantly increase viral load were mapped on developed, full length NP model, likely impacting interactions with host proteins and viral RNA.**

## INTRODUCTION

More than three years into the current pandemic of COVID-19, there are more questions than answers about the Severe Acute Respiratory Syndrome Coronavirus 2 (SARS-CoV-2). SARS-CoV-2 is spherical, enveloped, non-segmented, (+) sense RNA virus with a large ~30 kbs genome that despite its size shows remarkable ability to spread and mutate among human and animal populations.<sup>1–5</sup> The SARS-CoV-2 genome encodes nearly 30 proteins, including 4 structural, 15 non-structural and ~10 accessory proteins. The 4 structural proteins include: N (nucleocapsid, here abbreviated NP), S (spike; providing the “corona” of the virus), M (membrane) and E (envelope).<sup>6</sup> The SARS-CoV-2 structural proteins are essential.<sup>7</sup> The S protein, which facilitates receptor attachment and promotes membrane fusion, is the key target for neutralizing antibodies, and is the focus of current mRNA-based vaccines. Unfortunately, significant accumulation of mutations in this protein has the most pronounced impact on the efficacy of these vaccines.<sup>8–10</sup> The E protein contains hydrophobic N-terminal domain and C-terminal domain is required for viroporin formation and viral assembly. The M transmembrane protein possesses hydrophilic C-terminal and amphipathic N-terminal regions, and promotes spike incorporation and, through interaction with E and NP, it facilitates virion assembly.

NP, the most abundant viral protein, is essential for viral life cycle.<sup>11,12</sup> In the mature virus, the gRNA is covered by NP that protects RNA against hydrolysis. NP is critical for assembling viral gRNA and organizing it into ribonucleoprotein (RNP) complex for packaging into mature virion.<sup>13,14</sup> This is a crucial function of NP as a single break of gRNA chain makes it translationally inoperable. The NP is also essential for linking the viral genome to the viral membrane through interaction with the M protein.<sup>15</sup>

In SARS-CoV-2, NP, like other structural proteins and Orfs, is translated from subgenomic RNA (sgRNA)<sup>6,16</sup> coding for a 422-residues, 46 kDa protein. Betacoronavirus NPs share a common overall domain structure, with well-ordered N-terminal RNA-binding domain (NP<sup>RBD</sup>) and C-terminal dimerization domain (NP<sup>CTD</sup>).<sup>11,17</sup> These domains are linked by a serine-rich region, which contains several regulatory phosphorylation sites.<sup>18,19</sup> There are also unstructured regions on N- and C-termini of NP. Self-association of the full-length SARS-CoV-1 NP and the isolated NP<sup>CTD</sup> was initially demonstrated by yeast two-hybrid analysis, and the purified full-length protein was shown to self-associate into predominantly dimers as functional units in solution.<sup>20,21</sup> NP<sup>RBD</sup> binds genomic RNA to form RNP, while the NP<sup>CTD</sup> with disordered C-terminus promotes the dimerization of RNP,<sup>22–24</sup> as shown by the structure of SARS-CoV-2 NP<sup>CTD</sup> (PDB id: 6wjji).<sup>25</sup> The dimerization is followed by the formation of the higher-order RNP assemblies, but this process is not well understood. It likely involves cooperative interactions

<sup>1</sup>Center for Structural Biology of Infectious Diseases, Consortium for Advanced Science and Engineering, University of Chicago, Chicago, IL 60367, USA

<sup>2</sup>Structural Biology Center, X-ray Science Division, Argonne National Laboratory, Lemont, IL 60439, USA

<sup>3</sup>Data Science and Learning Division, Argonne National Laboratory, Lemont, IL 60439, USA

<sup>4</sup>Department of Biochemistry and Molecular Biology, University of Chicago, Chicago, IL 60367, USA

<sup>5</sup>Gale and Ira Drukier Institute for Children's Health, Weill Cornell Medicine, New York, NY 10021, USA

<sup>6</sup>Lead contact

\*Correspondence: [andrzej@anl.gov](mailto:andrzej@anl.gov)

<https://doi.org/10.1016/j.isci.2024.108976>



between the NP<sup>CTD</sup> and other viral proteins. Recent *in situ* cryoelectron tomography of SARS-CoV-2 virions has revealed a beads-on-a-string like arrangement of globular RNP complexes with local branching and stacks of helical filaments.<sup>13</sup>

Several other, non-structural functions have also been associated with the coronavirus NP.<sup>21</sup> This includes complement hyperactivation which may lead to collateral aggravated tissue injury having major impact on morbidity and mortality.<sup>26</sup> Complement is one of the first lines of defense in innate immunity and is essential for cellular integrity and tissue homeostasis, as well as for modifying the adaptive immune response. Moreover, NP proteolysis results in the formation of additional stable proteoforms that interact with host proteins.<sup>21</sup> Interestingly, the R203K + G204R mutations result in increased virus replication and higher-level viral RNA and protein expression both *in vitro* and *in vivo*. These mutations increase nucleocapsid phosphorylation and confer resistance to the inhibition of the host glycogen synthase kinase-3 (GSK-3).<sup>19</sup>

Even though the NP is located inside of the viral particle rather than on its surface, the excessive amount of it results in a very strong immune response in patients infected with SARS-CoV-1 and -CoV-2.<sup>27–29</sup> These patients show higher and earlier antibody responses to the NP than to S protein, or other viral proteins.<sup>28,30–32</sup> The NP elicits high titers of binding antibodies in humoral immune responses shortly after infection.<sup>31</sup> A possible explanation is that in host cells with actively replicating coronavirus there is a significant accumulation of NPs. This protein binds to various RNAs including viral gRNA, sgRNAs, and host RNAs. These factors provide a detection advantage over other coronavirus antigen targets and therefore NP is the main target for COVID-19 identification by antigen detection.

Surprisingly, there is very limited number of structures of coronavirus NP complexes with human antibodies available, particularly for SARS-CoV-2. To fill this gap and to better understand the SARS-CoV-2 NP structure, structural differences between NPs of related coronaviruses including SARS-CoV-1, potential presentation epitopes and antibody recognition we determined two structures of NP<sup>RBD</sup> and five structures of NP<sup>RBD</sup> complexes with SARS-CoV-2 NP-specific monoclonal antibodies (mAbs) derived from the COVID-19 convalescent patient. To understand the structure and function of SARS-CoV-2 NP we also modeled full-length NP, the NP dimer and complex with RNA. This modeling was aided by the available structures of the NP<sup>CTD</sup> domain of SARS-CoV-1 and CoV-2 and several related coronaviruses, AlphaFold models, and our own modeling efforts.

## RESULTS

### Crystal structures of N-terminal RNA-binding domain in two different crystal forms

The first two structures of SARS-CoV-2 NP<sup>RBD</sup> were determined in 2020 and immediately deposited to the Protein DataBank (PDB) to aid community efforts. The high-resolution structure was determined in the orthorhombic form at 1.70 Å (Table S1). There are four NP<sup>RBD</sup> monomers arranged in head-to-tail manner in the asymmetric unit. In chain A we modeled residues 50–173 and in chains B, C and D residues 49–173. Each monomer binds 2-(*N*-morpholino)-ethanesulfonic acid (MES), one chloride and one zinc ion, and one molecule of glycerol at the interface between two monomers (Figure 1; Table S1). The second NP<sup>RBD</sup> crystal belonged to monoclinic space group and diffracted X-rays to 2.67 Å resolution. This crystal also contains four NP<sup>RBD</sup> monomers and four zinc ions, but only two molecules of MES (Table S1). In chain A we modeled residues 51–173 (91–105 and 150–155 are disordered), in chain B residues 48–173 (93–101 are disordered), in chain C residues 50–173 (98–101 are disordered) and chain D residues 49–173 (93–102 are disordered). Nevertheless, collectively, these structures provide a continuous model of the protein from residue 48 to 173, including RNA binding region and key epitopes (Figure 1C) and represent one of the most complete NP<sup>RBD</sup> structure among coronavirus NP proteins (Figures 1A and 1B). The structures in two crystal forms show high level of similarity to each other (superimposition of chain A (PDB id: 6yvo) and chain C (PDB id: 6wkp)) yielded a root-mean-square deviation, r.m.s.d. of 0.48 Å across 116 C $\alpha$  atom pairs and to SARS-CoV-1 and MERS (r.m.s.d. 1.84 Å/120 C $\alpha$  atoms and 1.11 Å/120 C $\alpha$  atoms), respectively (Figures 1B and 1E). We used a high-resolution structure for a more detailed analysis. The structure of the NP<sup>RBD</sup> unit is made up of  $\beta$ -sheet involving five  $\beta$  strands ( $\beta_1$ , 56–57;  $\beta_2$ , 84–90;  $\beta_3$ , 107–113;  $\beta_6$ , 103–134;  $\beta_7$ , 170–172) with anti-parallel topology  $\beta_6 \uparrow \beta_2 \downarrow \beta_5 \uparrow \beta_1 \downarrow \beta_7 \uparrow$ . A protruding  $\beta$  hairpin (described as a palm region) is comprised of two strands ( $\beta_3$ , 93–95;  $\beta_4$ , 101–103), and opposite of the hairpin is a single  $3_{10}$ -helix ( $\eta_1$ , 79–82) (Figure 1D). The structure is very similar to a later deposited SARS-CoV-2 NP<sup>RBD</sup> structure (PDB id: 6m3m), which was also obtained from an orthorhombic crystal form with four NP<sup>RBD</sup> units per asymmetric unit.<sup>33</sup>

### Crystal structures of N-terminal RNA-binding domain/monoclonal antibodies complexes

Several mAbs were isolated using an antigen-bait sorting and single-cell sequencing approach from convalescent patients infected by SARS-CoV-2. Several mAbs were purified and characterized and structures of five complexes with NP<sup>RBD</sup> were determined, three at high resolution (NP<sup>RBD</sup>/S24-202 at 1.82 Å (PDB id: 7n3c), NP<sup>RBD</sup>/S24-1063 at 1.50 Å (PDB id: 7str), NP<sup>RBD</sup>/S24-1564 at 1.53 Å (PDB id: 7n3d), NP<sup>RBD</sup>/S24-188 at 2.90 Å (PDB id: 7sue), NP<sup>RBD</sup>/S24-1379 to 2.16 Å (PDB id: 7sts)) (Figure 3, Table S2). The NP<sup>RBD</sup> shows very similar conformation in all five complexes (r.m.s.d. of C $\alpha$  ~ 0.75 Å) and the structures are similar to free NP<sup>RBD</sup>, however some regions are disordered. The most complete are NP<sup>RBD</sup> structures in complexes with S24-202 (residues 44–173), S24-1063 (residues 44–172), and S24-1379 (residues 50–172). The mAbs sequences, both heavy (HC) and light chain (LC), are partly sequence conserved and showing quite large variability in complement-determining regions (CDRs) 1, 2 and 3 (Figure S1). The HC of S24-188 has a seven-residues insert prior to CDR3 compared to other mAbs in this study and that of S24-202 has a two-residue insertion.

In our structures the NP<sup>RBD</sup> and mAbs show very strong surface complementarity (Figure S2). Each mAb recognizes a different set of NP<sup>RBD</sup> epitopes (Figures 2 and 3A–3E). The structures revealed distinct CDRs for each mAbs complex with NP<sup>RBD</sup> (Figures 3A–3E and S3). Interestingly, most epitopes are partly shared but residues from RNA-binding surface are not included in interactions, potentially suggesting that epitope peptides are generated from the NP-RNA complex and that RNA protects some regions of NP from protease activity. S24-1564,

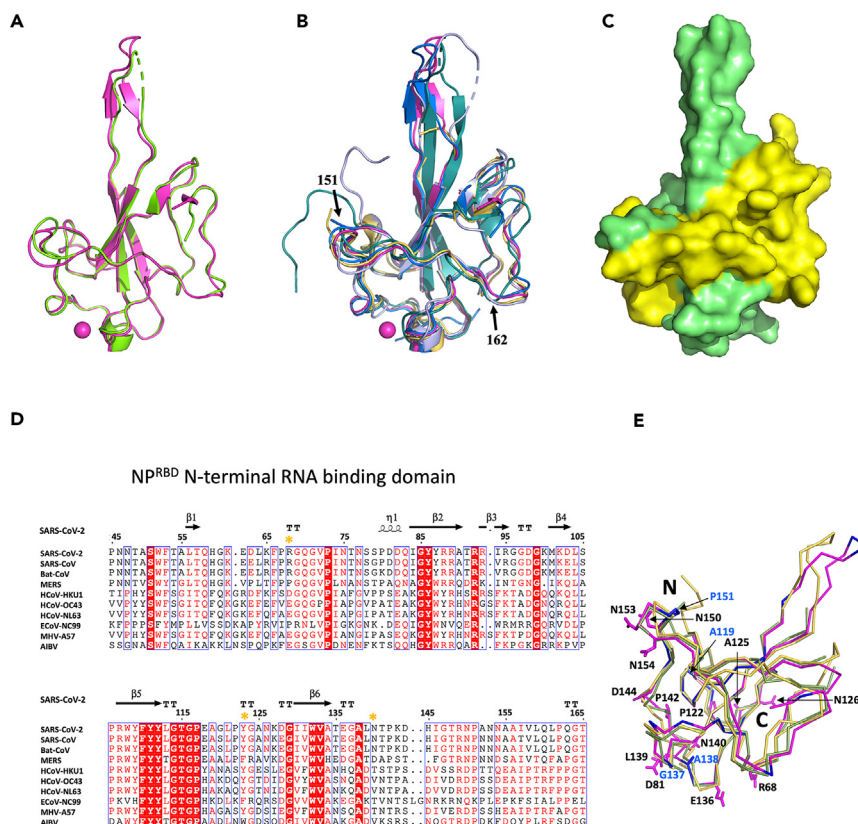


**Figure 1. Structure of protein NP<sup>RBD</sup> from SARS-CoV-2 and comparison of NPs from SARS-CoV-2, SARS-CoV-1 and MERS**

Two structures of NP<sup>RBD</sup> in two crystal forms – (A) orthorhombic (PDB id: 6vyo, 1.70 Å, magenta) and monoclinic (PDB id: 6wkp, 2.67 Å, green), these structures provide a complete model of the protein from residue 48 to 173, including RNA binding region and key epitopes.

(B) Comparison of NP<sup>RBD</sup> structures from SARS-CoV-2 (PDB id: 6vyo, magenta), SARS-CoV-1 (PDB id: 2ofz, blue), MERS (PDB id: 2kL2, yellow), HCoV-NL63 (PDB id: 5n4k, dark green), and HCoV-OC43 (PDB id: 4j3k, pale blue). Zinc ion is shown as a magenta sphere.

(C) NP<sup>RBD</sup> B- and T cell epitopes are conserved between SARS-CoV-1 and SARS-CoV-2: 48–69, 138–146, 153–173 (yellow surface) except for residues 63 (D/E), 65 (K/R), and 157 (I/T).

(D) Sequence alignment of NP<sup>RBD</sup> from SARS-CoV-2, SARS-CoV-1, MERS, HCoV-NL63, HCoV-OC53, Murine hepatitis virus A57, Avian infectious bronchitis virus (AIBV), and Equine Coronavirus NC99 (ECov-NC99): sequence numbering and secondary structure elements on top of sequence alignment are from the SARS-CoV-2 NP<sup>RBD</sup>. Yellow asterisks on top of the sequence indicate key residues recognized by mAbs.

(E) Superimposed structures shown in ribbon drawing: magenta for SARS CoV-2, light brown for SARS-CoV-1 and dark green for MERS. Conserved residues are indicated in red for sequence alignment and blue for the NP<sup>RBD</sup> structure (SARS-CoV-2). Residues involved in contacts with mAbs fragments are shown in stick drawing with the residue numbers labeled in black. The residue numbers for the conserved residues that are interacting with Fabs labeled in blue. \*\* Only a few conserved residues A119, G137, A138 and P151 are interacting with Fab.

S24–188, S24–202, and S24–1063 use epitope 136–144, however, involving different set of residues and few additional residues are shared between some mAbs (R68, D81). S24–1379 has a more divergent interactions than the others and uses exclusively 150–154 region. S24–1564, in addition to 136–140, binds residues from sequence 124–126. In all five cases, the protein is recognized specifically by residues from both heavy and light chains (Figures 3A–3E). S24–1063 is using a three-tyrosines motif for specific interactions (Figure S3) and has higher complementarity with SARS-CoV-2 NP<sup>RBD</sup> than other coronaviruses. Structure alignment of mAbs/SARS-CoV-2 NP<sup>RBD</sup> complex with SARS-CoV-1 NP<sup>RBD</sup> and with MERS NP<sup>RBD</sup> shows clashes or residues missing for interactions with mAbs (Figure S4). The interactions between mAbs and NP<sup>RBD</sup> involve hydrogen bonds, including some that are water mediated, salt bridges, and van der Waals contacts. High affinity and specificity are accomplished through contacts provided by residues coming from different CDRs (Figures 3A–3E, S1, and S3). For S24–1564, S24–1379, and S24–1063 residues from all three HC CDRs and two LC CDR1 and 3 contribute to binding (Figures 3B, 3C and 3D). For S24–188 only residues from HC CDR3, LC CDR1 and one non-CDR residues (R68) contribute to binding (Figure 3A) and for S24–202, only residues from HC CDR3 and two LC CDR1 and 3 contribute to binding (Figure 3E). There are some common and some very distinctive patterns. For example, all five antibodies use tyrosine residues to recognize NP<sup>RBD</sup>. S24–1063 uses a set of four (Figures 3G and S3) and S24–1564 a set of three tyrosine residues for recognition (Figure 3B). In contrast, S24–202 uses two arginine residues for binding (Figure 3F). For S24–188, 202, 1063 and 1564 the epitopes and specific amino acid sequence of interacting residues is conserved between SARS-CoV-1 and CoV-2 but MERS has several mutations

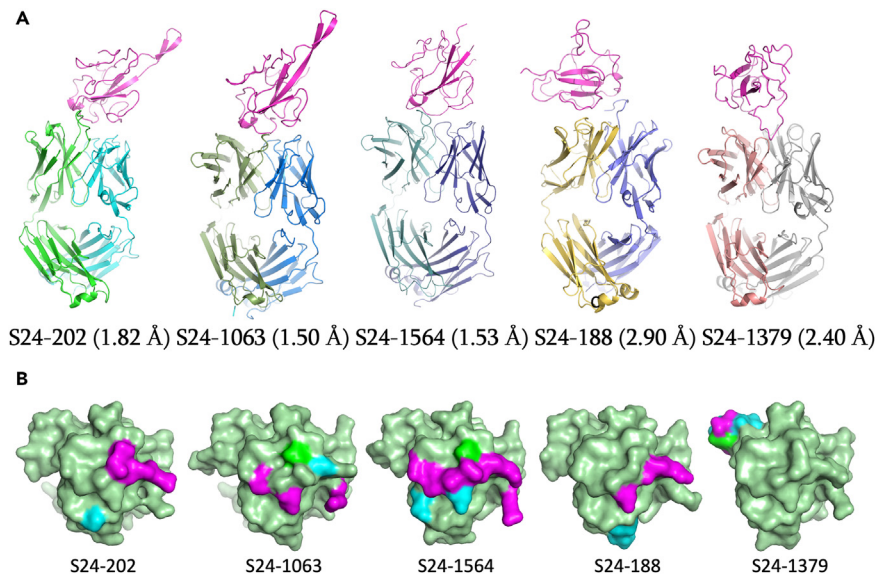


**Figure 2. Structures of NP<sup>RBD</sup> complexes with mAbs, epitopes of the RNA binding domain of NP and interactions between NP<sup>RBD</sup> and mAbs**  
(A) NPs in the complexes are shown in magenta. Light and heavy chains for each complex are shown in different color.  
(B) Overall NP<sup>RBD</sup> are shown in faded green and the epitopes interacting with CDR3 is indicated with magenta, green for CDR1, and cyan for CDR2.

and these mAbs may not cross-react. In contrast in S24-1379 complex interacting residues are very conserved and this mAb may cross react with SARS and MERS NPs.

We have compared interactions of mAbs and nanobodies (sdAbs) specifically recognizing NP<sup>RBD</sup> using structures available in PDB (Figure 4). The mAbs and sdAbs targeting the NP<sup>RBD</sup> show quite divergent epitopes, that nevertheless include known conserved NP<sup>RBD</sup> B- and T cell epitopes (Figure 1C). Except for mAbs S24-202, S24-1063, and S24-1564, which occupy the most common binding site, other mAbs and sdAbs exploit different surfaces of NP<sup>RBD</sup> in a manner that allow several pairs of mAbs and sdAbs simultaneously bind to the protein. Such complexes of mAbs were described previously for SARS-CoV-2 NP<sup>RBD</sup>.<sup>30</sup> Interestingly, the antibody and nanobody interactions seem to exclude single and double-stranded RNA binding surfaces (Figure 4).

### Modeling full length SARS-CoV-2 nucleocapsid protein reveal surfaces for interactions

The obligate homodimeric structure of NP<sup>CTD</sup> domain and other work suggested that the downstream unstructured tail mediates further self-association into tetramer, hexamer, and potentially higher oligomeric forms that can enhance RNA-binding and virion assembly and potentially enhance infectivity.<sup>23</sup> Other studies have suggested that the protein's N-terminal region, including the RNA-binding domain, can also self-associate, highlighting the possibility that assembly of full-length nucleocapsid is mediated by cooperative interactions among several interfaces and RNA.<sup>24</sup> One critical step in coronavirus replication is the assembly of the viral genomic RNA and N protein into an RNP complex, which in betacoronaviruses forms a helical filament structure that accumulates at the curved membrane and is packaged into virions through interactions of its C-terminal domain with the M membrane protein.<sup>34</sup> Here, we show a model of SARS-CoV-2 nucleocapsid as an intertwined dimer similar to that of related betacoronaviruses (Figure 5). To generate full length dimeric N protein, we used a combination of known X-ray and NMR structures, including complexes with RNA and AF2 predicted and simulated model. We mapped on this dimer mutated residues identified in the omicron variant that significantly increased SARS-CoV-2 virulence.<sup>35</sup> Our 3D models present protein surfaces available for potential interactions that can be exploited in antibody and vaccine development. The assembly of NP dimers into higher-order helical filaments is not well understood, but likely involves cooperative interactions between the dimerization domain and other regions of the protein, plus the bound RNA but it seems that higher-order assembly requires both the dimerization domain and the extended, disordered C-terminus of the protein. Together with previously published work it reveals the structure and RNA-binding properties, assembly, and higher order architecture of the nucleocapsid.

### Molecular simulation reveals the antibody/antigen interfacial dynamics

We then simulated the antibody binding NP<sup>RBD</sup> structures to understand antibody binding selectivity on the epitope domains. The simulation results are summarized using root-mean-square fluctuation (RMSF) and number of antibody residues that NP<sup>RBD</sup> is contacting with (cutoff at 10 Å), as shown in Figure 6. S24-202 and S24-1063 show a similar chain fluctuation, and S24-1379 show a divergent pattern in both chain fluctuation and multimer stacking. From the RMSF profile, the largest chain fluctuation is identified at the long  $\beta$ -hairpin, around residue Asp98. It binds with the viral RNA, as shown in two NMR structures (PDB ids: 7act and 7acs), and is destabilized in the solvent environment, partially assuming loop structure. The S24-202 and S24-1063 form a contacting interface with the 136–144 epitope of NP<sup>RBD</sup> with both the light

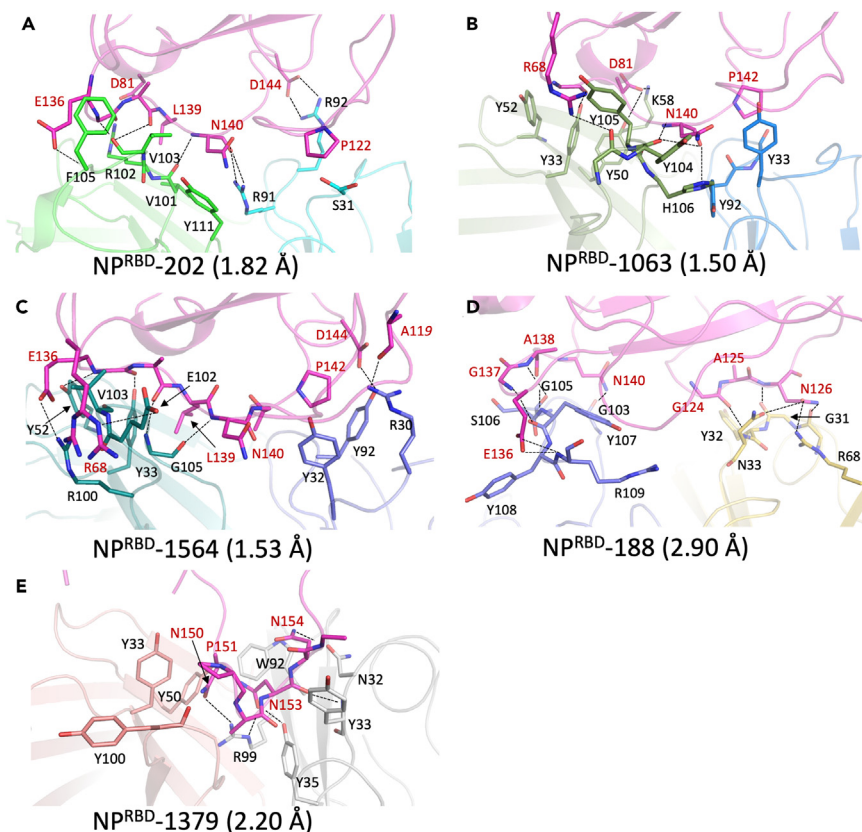


**Figure 3. Specific interactions between NP<sup>RBD</sup> and mAbs**

(A–E) Details of interaction between NP<sup>RBD</sup> and mAbs. NP<sup>RBD</sup> is shown in magenta, magenta residues in sticks are involved in interactions with mAbs, hydrophilic interactions (i.e., H-bonds) are shown in dotted lines, others are for hydrophobic (van der Waals) interactions. Heavy chains and light chains of mAbs are indicated in different colors and the interacting residues are shown in sticks.

and heavy chains. The residues 136–140 are binding with the heavy chain and residues 140–144 with the light chain. In addition, NP<sup>RBD</sup> also binds with mainly the light chain using residues 120–123, and exclusively with the heavy chain involving residues Gln70 and Pro80, with lower contacting occurrence.

The NP<sup>RBD</sup>/S24-1379 complex shows a completely different binding profile as the result of the packing of two antibody/antigen pairs. We focus on chain C NP<sup>RBD</sup> that binds with both antibodies and its counterpart NP<sup>RBD</sup> in the dimer, labeled as chain D. The two antibodies are tagged based on their number of contacts with chain C. The primary antibody is labeled with chain H and L for its heavy and light chain, respectively, and the secondary with chain H<sub>1</sub> and L<sub>1</sub>. The primary epitope at the binding interface involves residues 150–154, the same as it in the crystal structure. It binds with both the primary heavy and light chains of S24-1379. There is also contact around residue Pro117 of NP<sup>RBD</sup> with the antibody heavy chain. Moreover, the NP<sup>RBD</sup> also contacts with the second antibody/antigen pair in the dimer. It mainly contacts with its counterpart NP<sup>RBD</sup>, chain D, and the secondary light chain, chain L<sub>1</sub>. Notably, the NP<sup>RBD</sup> residues 157–166, bound to chain D, is within one of the well-established epitopes, 153–173. Contacts are also found around residues 74–80, between the NP<sup>RBD</sup> and both chains D and L<sub>1</sub>.

This antibody binding suppresses the local chain fluctuations of NP<sup>RBD</sup>, with stable binding between the antibody and antigen. Lower RMSF is found at the binding regions. For example, the 150–154 and 74–80 domains of NP<sup>RBD</sup>/S24-1379 show much lower RMSFs than those of NP<sup>RBD</sup>/S24-1564 and NP<sup>RBD</sup>/S24-1063, due to the binding interface. Comparing with the result from the simulation of full-length NP, the antibody bound NP<sup>RBD</sup>s show lower RMSF as well (Figure S5). The binding of antibody disrupts the natural dynamic fluctuation of the NP<sup>RBD</sup> domain.

## DISCUSSION

The two NP<sup>RBD</sup> structures are very similar to SARS-CoV-1 (PDB id: 2ofz), MERS-CoV (PDB id: 6kL2), HCoV-NL63 (PDB id: 5n4k), and HCoV-OC43 (PDB id: 4j3k), which are 92%, 59%, 46%, and 46% identical, respectively in the NP<sup>RBD</sup> region. Although some parts of the structure show different conformations (N- and C-termini, orientation of palm region) some others show remarkable conformational conservation (for example region 151–162 as indicated with two arrows in Figure 1B). Our structures are also similar to the NMR structure of the SARS-CoV-1 NP<sup>RBD</sup>.<sup>36</sup> Thus, while SARS-CoV-2 NP<sup>RBD</sup> shares relatively low sequence similarity with other coronaviral NPs, the core topology is conserved and like that of other RNA binding proteins (Figures 1D and 1E).

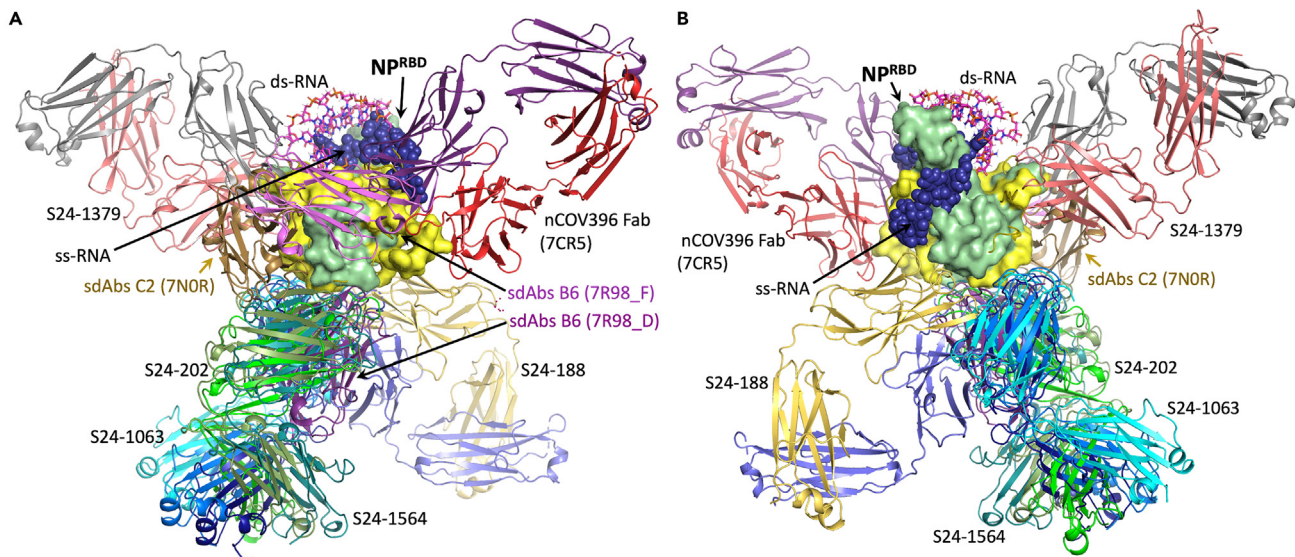


**Figure 4. The mAbs and nanobodies (sdAbs) targeting the NP<sup>RBD</sup> common but more divergent epitopes**

mAbs and nanobodies (sdAbs) exploit and bind different sites of NP<sup>RBD</sup> except for mAbs S24-202, S24-1063, and S24-1564 which occupy the most common site. However, RNA (ds or ss) binding site is not a part of this epitope. Every chain of antibody fragments binding to NP<sup>RBD</sup> are labeled and colored differently, ds-RNA (magenta) and ss-RNA (purple) from the structures of PDB ids 7acs and 7act respectively, are indicated by sticks and spheres, respectively. NP<sup>RBD</sup> is shown in fade green surface and the conserved NP<sup>RBD</sup> B- and T cell epitopes is shown in yellow surface. (A) represent front view and (B) back view of the structure.

The SARS-CoV-2 NP protein has several well-established epitope regions (45–69, 89–104, 138–146, 153–173, 185–197, 277–287 and 378–390).<sup>37–39</sup> The first four are present in NP<sup>RBD</sup> and they are moderately conserved among multiple  $\alpha/\beta$  coronaviruses strains including SARS-CoV-1 and MERS (Figure 1D). This suggests a common origin and potential pre-existing immunity. The immune response is complex and is evolving as host adaptation is detected. Noticeable maturation of non-neutralizing, non-protective antibodies to nucleocapsid and ORF8 is observed over time. This highlights the need for periodic vaccination to stimulate the production of spike-specific neutralizing mAbs.<sup>28</sup>

Structural biology plays an important role in addressing challenges created by emerging pathogens globally, as it was shown for COVID-19 pandemic. Structural genomics programs developed high-throughput protein production pipelines capable of generating reagents for biochemical and biophysical characterization. During the COVID-19 pandemic, these reagents were rapidly produced and shared with biology community. Structure determination pipelines using X-ray crystallography with synchrotron radiation and by electron microscopy using cryo-EM facilities quite rapidly determined structures of many proteins and complexes from the emerging pathogen. These efforts supported functional studies, helped identifying small molecule leads for therapeutics and antibodies for diagnostics and treatments.<sup>30,40–42</sup> In fact, our studies contributed to the 4-fold improvement of nucleocapsid detection for application in lateral flow diagnostic tests.<sup>30,40–42</sup> Importantly, in the spirit of collaboration, all data were shared enabling high-performance computational analysis and application artificial intelligence and machine learning approaches for drug discovery. Structural biology teams established highly productive collaborations that resulted in important contributions to fight pandemic. However, this was still too slow and there are significant challenges to tackle and considerably improve response to future pandemics.

Structural characterization of human mAbs complexes with NP provide basis for identifying interactions and may be crucial for early diagnosis of SARS-CoV-2 and other pathogens. As such, a better understanding of the SARS-CoV-2 NP's structure, and structural differences between it and NPs of related coronaviruses including SARS-CoV-1, may aid the development of sensitive and specific immunological tests.

Our structures provide high quality model of NP<sup>RBD</sup> obtained under different conditions and crystal packing environment. This domain is very stable and shows a well-defined fold. Zinc binding was observed in both crystal forms. Conserved epitopes are presented on the protein surface, but they do not overlap with RNA binding surface. Structures of complexes of mAbs with NP<sup>RBD</sup> revealed distinct CDRs from both HC and LC for each mAbs complex. CDR1-3 of these mAbs are diverse but bind the same NP<sup>RBD</sup>, using similar epitopes. The mAbs interact with NP<sup>RBD</sup> using the residues from different regions of HC and LC. The overall conformation of NP<sup>RBD</sup> in the complexes are quite similar, however, the orientations of NP<sup>RBD</sup> in the complexes relative to mAbs can be dramatically different (Figure 2).

NP<sup>RBD</sup> in complex with S24-1379 utilizes a distinct, more divergent epitope than the other complexes, which shares most parts of epitopes, including residues 136–140. Interactions involve hydrophobic contacts, direct and water mediated hydrogen bonds and salt bridges. The epitope of residues 136–142 is buried at the dimer interface but other epitopes residues 124–126 identified only for Fab S24-188 and residues 151–154 for S24-1379 are exposed. Conservation of epitopes sequences suggests that some isolated mAbs may cross react with SARS and MERS NPs. Our data show that more than one antibody can bind simultaneously to SARS-CoV-2 NP<sup>RBD</sup> as was reported previously.<sup>30</sup> This can increase detection sensitivity level.

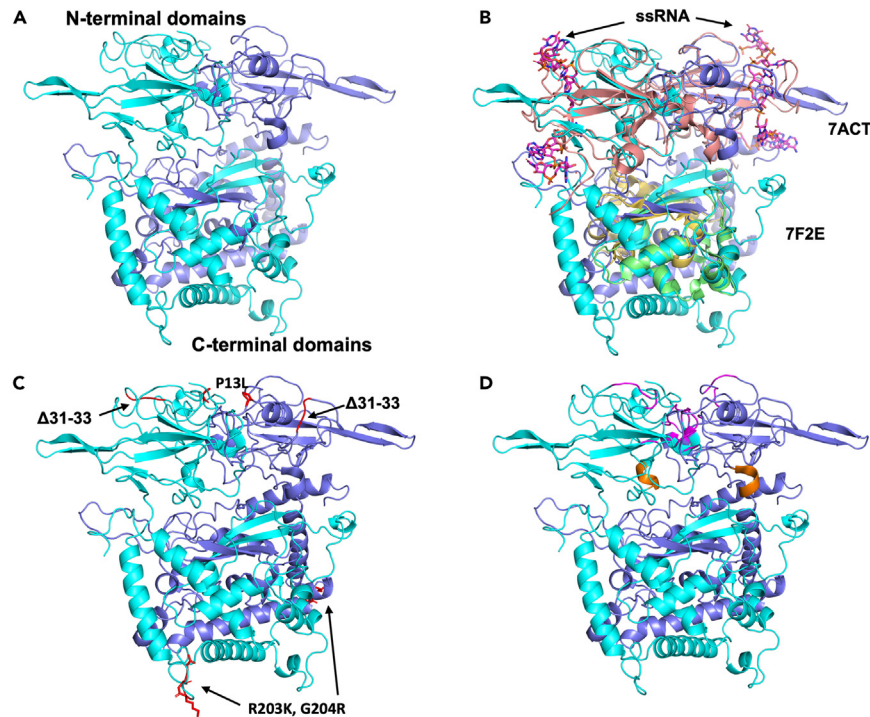


**Figure 5. Model of full-length SARS-CoV-2 NP dimer in complex with RNA**

(A) The dimeric AF2 predicted and simulated full-length SARS-CoV-2 NP model (cyan and dark blue) is shown. For AF2 model prediction, the NMR structure of the NP<sup>RBD</sup> of the NP in the complex with 10 base-ssRNA (PDB id: 7act) was used as a template.

(B) The NP model (in cyan and dark blue) is superimposed with the structures of NP<sup>RBD</sup> in the complex with single stranded RNA (PDB id: 7act) (orange) and the dimer of the C-terminal domains (light green and light yellow) (PDB id: 7f2e). RMSD of matching Ca atoms (105) of monomers is 1.49 Å for the NP<sup>RBD</sup> and 1.12 Å for matching 185 Ca atoms from dimers between NP<sup>CTD</sup>. The ssRNA are also shown in magenta sticks.

(C) Mutated residues identified in the omicron variant are indicated on the model: P13L, R203K and G204R in red sticks, deletion mutations ( $\Delta$ 31-33) are shown in red on the cartoon drawing.

(D) The epitopes recognized by 5 Fabs are indicated in magenta and orange (found only in the NP<sup>RBD</sup>/S24-1379 structure) on the NP<sup>RBD</sup> of both monomers of the model. The epitope of residues 136–142 is buried at the dimer interface but other epitopes residues 124–126 identified only for Fab S24-188 and residues 151–154 for S24-1379 are exposed.

The full-length model of SARS-CoV-2 NP dimer and its complex with RNA allow to explain several previously reported results. It was observed that several NP residues - P13L, and deletion  $\Delta$ 31-33 - when mutated in the omicron variant significantly increase virus proliferation. In the dimer of full-length NP these are located close to RNA binding surface (P13L and  $\Delta$ 31-33) and on the opposite site of the dimer most likely involved in formation higher order assembly. The MD simulations reveal dynamics of mAb-NP interactions including the conformational landscape and transitions. Antibody binding to NP<sup>RBD</sup> attenuates the natural dynamic fluctuation.

It appears that mAbs can also bind to NP/RNA complex as epitopes seems accessible for mAbs. Structural characterization of human mAbs complexes with NP<sup>RBD</sup> provide a basis for understanding interactions and may be crucial for early diagnosis of SARS-CoV-2 and other pathogens. The overall conformations of NP<sup>RBD</sup> in all the complexes are similar. The mAbs and sdAbs binding to the NP<sup>RBD</sup> recognize quite divergent epitopes allowing for pairs of antibodies to bind as it was reported previously (Figure 4).<sup>30,40–42</sup> Interestingly, human NP targeting mAbs from COVID-19 convalescents play essential roles in the inhibition of complement hyperactivation.<sup>26</sup>

### Limitations of the study

This study presents structures of SARS-CoV-2 nucleocapsid N-terminal domain and its complexes with human antibodies. Although we made several attempts, we failed to obtain crystal structure of the full length of the NP, therefore we resorted to produce computational models that include NP<sup>RBD</sup>, NP<sup>CTD</sup> and the linker. Future experimental structures may improve these models. We also provide a dimer model. Some parts of our structures are poorly ordered or completely disordered. Our structures also are missing phosphorylation sites that are important for some protein activities. It is not clear what is the role of zinc ions, and more studies are needed. Based on the sequence conservation and structural similarity presented here, we hypothesize that human antibodies may cross-react with SARS and MERS nucleocapsid targets, but we do not have direct evidence and further characterization is needed.

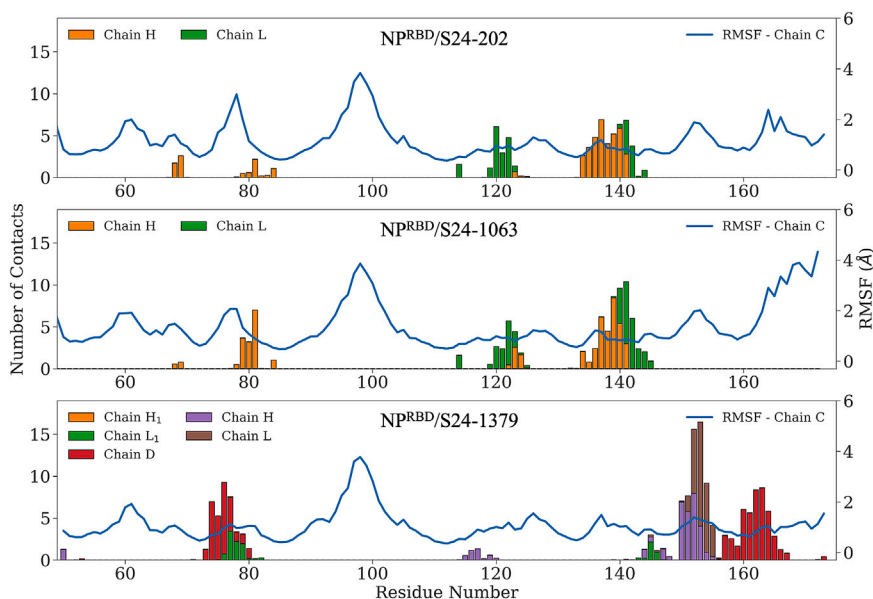


**Figure 6. MD simulations indicate distinct access of conformational states for NP-mAb complexes**

The RMSFs of NP<sup>RBD</sup> (Chain C) are calculated while binding with different antibodies. The number of contacts between NP<sup>RBD</sup> and different antibody chains are shown in bars. The binding/contacting with antibody constrains the chain fluctuation of NP<sup>RBD</sup>. The NP<sup>RBD</sup>/S24-1379 shows a completely different binding profile for it consists of two set of antibody/antigen pairs.

## STAR★METHODS

Detailed methods are provided in the online version of this paper and include the following:

- KEY RESOURCES TABLE
- RESOURCE AVAILABILITY
  - Lead contact
  - Materials availability
  - Data and code availability
  - Human samples
- EXPERIMENTAL MODEL AND STUDY PARTICIPANT DETAILS
- METHOD DETAILS
  - Gene cloning, protein expression and purification of NP<sup>RBD</sup>
  - Preparation of mAbs/NP<sup>RBD</sup> complexes for crystallization
  - Crystallization experiments
  - Data collection, structure determination and refinement
  - AlphaFold and molecular dynamics simulations

## SUPPLEMENTAL INFORMATION

Supplemental information can be found online at <https://doi.org/10.1016/j.isci.2024.108976>.

## ACKNOWLEDGMENTS

We truthfully thank the members of the SBC at Argonne National Laboratory, especially Alex Lavens and Krzysztof Lazarski for their help with setting beamline and data collection, and Paula Bulaon for help in preparing this article. Funding for this project was provided in part by federal funds from the National Institute of Allergy and Infectious Diseases, National Institutes of Health, Department of Health and Human Services, under Contracts HHSN272201700060C and 75N93022C00035 (AJ), the Collaborative Influenza Vaccine Innovation Centers (CIVIC; 75N93019C00051, PCW) and Award Number P01AI165077 (AJ, PCW) and by the DOE Office of Science through the National Virtual Biotechnology Laboratory, a consortium of DOE national laboratories focused on response to COVID-19, with funding provided by the Coronavirus CARES Act (AJ) and by the U.S. Department of Energy, Offices of Basic Energy Sciences and Advanced Scientific Computing Research through the Biopreparedness Research Virtual Environment (BRaVE) under contract number DE-AC02-O5CH11231 and specifically to Taskforce 5 (DOE-BRaVET5). Results shown in this report are derived from work performed at SBC funded by the U.S. Department of Energy,

Office of Biological and Environmental Research and operated for the DOE Office of Science at the Advanced Photon Source by Argonne National Laboratory under Contract No. DE-AC02-06CH11357. The content is solely the responsibility of the authors and does not necessarily represent the official views of the National Institutes of Health.

### AUTHOR CONTRIBUTIONS

A.J., P.W., and Y.K., initiated the project. R.J., cloned initial constructs, expressed, and purified the first batch of protein. M.E. continued with different constructs, and complexes. H.L.D., H.M., C.T.S., L.L., S.C., N.Y.Z., isolated specific B-cells, identified mAbs, sequenced mAbs genes, overexpressed and purified Fabs. N.M., C.T. purified protein and crystallized complexes with mAbs. Y.K., N.M., and C.C., collected and analyzed diffraction data. Y.K. and C.C., determined, refined, and, together with K.M., and A.J., analyzed structures. M.H., and A.R., performed modeling and computer simulation experiments, and model analysis. Finally, Y.K., A.R., P.W., and A.J., conceived and directed the research as well as wrote the article.

### DECLARATION OF INTERESTS

The authors declare no competing interests.

Received: September 8, 2023

Revised: November 2, 2023

Accepted: January 16, 2024

Published: January 19, 2024

### REFERENCES

- Cao, C., Cai, Z., Xiao, X., Rao, J., Chen, J., Hu, N., Yang, M., Xing, X., Wang, Y., Li, M., et al. (2021). The architecture of the SARS-CoV-2 RNA genome inside virion. *Nat. Commun.* **12**, 3917.
- Hao, Y.-J., Wang, Y.L., Wang, M.Y., Zhou, L., Shi, J.Y., Cao, J.M., and Wang, D.P. (2022). The origins of COVID-19 pandemic: A brief overview. *Transbound. Emerg. Dis.* **69**, 3181–3197.
- Reis, J., Faou, A.L., Buguet, A., Sandner, G., and Spencer, P. (2022). Covid-19: Early Cases and Disease Spread. *Ann. Glob. Health* **88**, 83.
- Wiegand, T., Nemudryi, A., Nemudraia, A., McVey, A., Little, A., Taylor, D.N., Walk, S.T., and Wiedenheft, B. (2022). The Rise and Fall of SARS-CoV-2 Variants and Ongoing Diversification of Omicron. *Viruses* **14**, 2009.
- Frazzini, S., Amadori, M., Turin, L., and Riva, F. (2022). SARS CoV-2 infections in animals, two years into the pandemic. *Arch. Virol.* **167**, 2503–2517.
- Kim, D., Lee, J.Y., Yang, J.S., Kim, J.W., Kim, V.N., and Chang, H. (2020). The Architecture of SARS-CoV-2 Transcriptome. *Cell* **181**, 914–921.e10.
- Satarker, S., and Nampoothiri, M. (2020). Structural Proteins in Severe Acute Respiratory Syndrome Coronavirus-2. *Arch. Med. Res.* **51**, 482–491. <https://www.sciencedirect.com/science/article/pii/S018844092030727X>.
- Abulsoud, A.I., El-Husseiny, H.M., El-Husseiny, A.A., El-Mahdy, H.A., Ismail, A., Elkhawaga, S.Y., Khidir, E.G., Fathi, D., Mady, E.A., Najda, A., et al. (2023). Mutations in SARS-CoV-2: Insights on structure, variants, vaccines, and biomedical interventions. *Biomed. Pharmacother.* **157**, 113977. <https://www.sciencedirect.com/science/article/pii/S075333222201366X>.
- Peng, Q., Zhou, R., Liu, N., Wang, H., Xu, H., Zhao, M., Yang, D., Au, K.K., Huang, H., Liu, L., and Chen, Z. (2022). Naturally occurring spike mutations influence the infectivity and immunogenicity of SARS-CoV-2. *Cell. Mol. Immunol.* **19**, 1302–1310.
- Romeo, I., Prandi, I.G., Giombini, E., Gruber, C.E.M., Pietrucci, D., Borocci, S., Abid, N., Fava, A., Beccari, A.R., Chillemi, G., and Talarico, C. (2022). The Spike Mutants Website: A Worldwide Used Resource against SARS-CoV-2. *Int. J. Mol. Sci.* **23**, 13082.
- Zhang, B., Tian, J., Zhang, Q., Xie, Y., Wang, K., Qiu, S., Lu, K., and Liu, Y. (2022). Comparing the Nucleocapsid Proteins of Human Coronaviruses: Structure, Immunoregulation, Vaccine, and Targeted Drug. *Front. Mol. Biosci.* **9**, 761173.
- Wu, C., Qavi, A.J., Hachim, A., Kaviani, N., Cole, A.R., Moyle, A.B., Wagner, N.D., Sweeney-Gibbons, J., Rohrs, H.W., Gross, M.L., et al. (2020). Characterization of SARS-CoV-2 N protein reveals multiple functional consequences of the C-terminal domain. Preprint at bioRxiv. 2020.11.30.404905. <http://biorxiv.org/content/early/2020/11/30/2020.11.30.404905.abstract>.
- Klein, S., Cortese, M., Winter, S.L., Wachsmuth-Melm, M., Neufeldt, C.J., Cerikan, B., Stanifer, M.L., Boulant, S., Bartenschlager, R., and Chlanda, P. (2020). SARS-CoV-2 structure and replication characterized by in situ cryo-electron tomography. *Nat. Commun.* **11**, 5885.
- Zinzula, L., Beck, F., Klumpe, S., Bohn, S., Pfeifer, G., Bollschweiler, D., Nagy, I., Plietzko, J.M., and Baumeister, W. (2021). Cryo-EM structure of the cetacean morbillivirus nucleoprotein-RNA complex. *J. Struct. Biol.* **213**, 107750. <https://www.sciencedirect.com/science/article/pii/S1047847721000551>.
- Dinesh, D.C., Chalupska, D., Silhan, J., Koutna, E., Nencka, R., Veverka, V., and Boura, E. (2020). Structural basis of RNA recognition by the SARS-CoV-2 nucleocapsid phosphoprotein. *PLoS Pathog.* **16**, e1009100.
- Alexandersen, S., Chamings, A., and Bhatta, T.R. (2020). SARS-CoV-2 genomic and subgenomic RNAs in diagnostic samples are not an indicator of active replication. *Nat. Commun.* **11**, 6059.
- Ma, Y., Tong, X., Xu, X., Li, X., Lou, Z., and Rao, Z. (2010). Structures of the N- and C-terminal domains of MHV-A59 nucleocapsid protein corroborate a conserved RNA-protein binding mechanism in coronavirus. *Protein & Cell* **1**, 688–697.
- Luo, H., Ye, F., Chen, K., Shen, X., and Jiang, H. (2005). SR-Rich Motif Plays a Pivotal Role in Recombinant SARS Coronavirus Nucleocapsid Protein Multimerization. *Biochemistry* **44**, 15351–15358.
- Johnson, B.A., Zhou, Y., Lokugamage, K.G., Vu, M.N., Bopp, N., Crocquet-Valdes, P.A., Kalveram, B., Schindewolf, C., Liu, Y., Scharton, D., et al. (2022). Nucleocapsid mutations in SARS-CoV-2 augment replication and pathogenesis. *PLoS Pathog.* **18**, e1010627.
- Yu, I.M., Gustafson, C.L.T., Diao, J., Burgner, J.W., 2nd, Li, Z., Zhang, J., and Chen, J. (2005). Recombinant Severe Acute Respiratory Syndrome (SARS) Coronavirus Nucleocapsid Protein Forms a Dimer through Its C-terminal Domain. *J. Biol. Chem.* **280**, 23280–23286.
- Lutowski, C.A., El-Baba, T.J., Bolla, J.R., and Robinson, C.V. (2021). Multiple Roles of SARS-CoV-2 N Protein Facilitated by Proteoform-Specific Interactions with RNA, Host Proteins, and Convalescent Antibodies. *JACS Au* **1**, 1147–1157.
- Khan, W.H., Khan, N., Mishra, A., Gupta, S., Bansode, V., Mehta, D., Bhambure, R., Ansari, M.A., Das, S., and Rathore, A.S. (2022). Dimerization of SARS-CoV-2 nucleocapsid protein affects sensitivity of ELISA based diagnostics of COVID-19. *Int. J. Biol. Macromol.* **200**, 428–437. <https://www.sciencedirect.com/science/article/pii/S014181302200109X>.
- Zhao, H., Nguyen, A., Wu, D., Li, Y., Hassan, S.A., Chen, J., Shroff, H., Piszczek, G., and Schuck, P. (2022). Plasticity in structure and assembly of SARS-CoV-2 nucleocapsid protein. *PNAS Nexus* **1**, pgac049.

24. Ye, Q., West, A.M.V., Silletti, S., and Corbett, K.D. (2020). Architecture and self-assembly of the SARS-CoV-2 nucleocapsid protein. *Protein Sci.* 29, 1890–1901.
25. Vandervaart, J.P., Inniss, N.L., Ling-Hu, T., Minasov, G., Wiersum, G., Rosas-Lemus, M., Shuvalova, L., Achenbach, C.J., Hultquist, J.F., Satchell, K.J.F., and Bachtta, K.E.R. (2023). Serodominant SARS-CoV-2 Nucleocapsid Peptides Map to Unstructured Protein Regions. *Microbiol. Spectr.* 11, e0032423-23.
26. Kang, S., Yang, M., He, S., Wang, Y., Chen, X., Chen, Y.Q., Hong, Z., Liu, J., Jiang, G., Chen, Q., et al. (2021). A SARS-CoV-2 antibody curbs viral nucleocapsid protein-induced complement hyperactivation. *Nat. Commun.* 12, 2697.
27. Leung, D.T.M., Tam, F.C.H., Ma, C.H., Chan, P.K.S., Cheung, J.L.K., Niu, H., Tam, J.S.L., and Lim, P.L. (2004). Antibody Response of Patients with Severe Acute Respiratory Syndrome (SARS) Targets the Viral Nucleocapsid. *J. Infect. Dis.* 190, 379–386.
28. Dugan, H.L., Stamper, C.T., Li, L., Changrob, S., Asby, N.W., Halfmann, P.J., Zheng, N.Y., Huang, M., Shaw, D.G., Cobb, M.S., et al. (2021). Profiling B cell immunodominance after SARS-CoV-2 infection reveals antibody evolution to non-neutralizing viral targets. *Immunity* 54, 1290–1303.e7.
29. Hachim, A., Gu, H., Kavian, O., Kwan, M.Y., Chan, W.H., Yau, Y.S., Chiu, S.S., Tsang, O.T., Hui, D.S., Ma, F., Lau, E.H., et al. (2021). The SARS-CoV-2 antibody landscape is lower in magnitude for structural proteins, diversified for accessory proteins and stable long-term in children. Preprint at medRxiv. 2021.01.03. 21249180. <http://medrxiv.org/content/early/2021/01/04/2021.01.03.21249180.1.abstract>.
30. Hodge, C.D., Rosenberg, D.J., Grob, P., Wilamowski, M., Joachimiak, A., Hura, G.L., and Hammel, M. (2021). Rigid monoclonal antibodies improve detection of SARS-CoV-2 nucleocapsid protein. *mAbs* 13, 1905978.
31. Che, X.-Y., Hao, W., Wang, Y., Di, B., Yin, K., Xu, Y.C., Feng, C.S., Wan, Z.Y., Cheng, V.C.C., and Yuen, K.Y. (2004). Nucleocapsid Protein as Early Diagnostic Marker for SARS. *Emerg. Infect. Dis.* 10, 1947–1949. [https://wwwnc.cdc.gov/eid/article/10/11/04-0516\\_article](https://wwwnc.cdc.gov/eid/article/10/11/04-0516_article).
32. Li, T., Wang, L., Wang, H., Li, X., Zhang, S., Xu, Y., and Wei, W. (2020). Serum SARS-COV-2 Nucleocapsid Protein: A Sensitivity and Specificity Early Diagnostic Marker for SARS-COV-2 Infection. *Front. Cell. Infect. Microbiol.* 10, 470.
33. Kang, S., Yang, M., Hong, Z., Zhang, L., Huang, Z., Chen, X., He, S., Zhou, Z., Zhou, Z., Chen, Q., et al. (2020). Crystal structure of SARS-CoV-2 nucleocapsid protein RNA binding domain reveals potential unique drug targeting sites. *Acta Pharm. Sin. B* 10, 1228–1238. <https://www.sciencedirect.com/science/article/pii/S2211383520305505>.
34. Wang, X., Yang, Y., Sun, Z., and Zhou, X. (2023). Crystal structure of the membrane (M) protein from a bat betacoronavirus. *PNAS Nexus* 2, pgad021.
35. Syed, A.M., Ciling, A., Taha, T.Y., Chen, I.P., Khalid, M.M., Sreekumar, B., Chen, P.Y., Kumar, G.R., Suryawanshi, R., Silva, I., et al. (2022). Omicron mutations enhance infectivity and reduce antibody neutralization of SARS-CoV-2 virus-like particles. *Proc. Natl. Acad. Sci. USA* 119, e2200592119.
36. Huang, Q., Yu, L., Petros, A.M., Gunasekera, A., Liu, Z., Xu, N., Hajduk, P., Mack, J., Fesik, S.W., and Olejniczak, E.T. (2004). Structure of the N-Terminal RNA-Binding Domain of the SARS CoV Nucleocapsid Protein. *Biochemistry* 43, 6059–6063.
37. Forcelloni, S., Benedetti, A., Dilucca, M., and Giansanti, A. (2021). Identification of Conserved Epitopes in SARS-CoV-2 Spike and Nucleocapsid Protein. *Curr. Genom.* 22, 541–549.
38. Lee, J.-H., Jung, Y., Lee, S.K., Kim, J., Lee, C.S., Kim, S., Lee, J.S., Kim, N.H., and Kim, H.G. (2022). Rapid Biosensor of SARS-CoV-2 Using Specific Monoclonal Antibodies Recognizing Conserved Nucleocapsid Protein Epitopes. *Viruses* 14, 255.
39. Rodrigues-da-Silva, R.N., Conte, F.P., da Silva, G., Carneiro-Alencar, A.L., Gomes, P.R., Kuriyama, S.N., Neto, A.A.F., and Lima-Junior, J.C. (2023). Identification of B-Cell Linear Epitopes in the Nucleocapsid (N) Protein B-Cell Linear Epitopes Conserved among the Main SARS-CoV-2 Variants. *Viruses* 15, 923.
40. Guerra, D., Beaumont, T., Radić, L., Kerster, G., van der Straten, K., Yuan, M., Torres, J.L., Lee, W.H., Liu, H., Poniman, M., et al. (2023). Broad SARS-CoV-2 neutralization by monoclonal and bispecific antibodies derived from a Gamma-infected individual. *iScience* 26, 108009. <https://www.sciencedirect.com/science/article/pii/S2589004223020862>.
41. Torres, J.L., Ozorowski, G., Andreano, E., Liu, H., Coppis, J., Piccini, G., Donnici, L., Conti, M., Planchais, C., Planas, D., et al. (2022). Structural insights of a highly potent pan-neutralizing SARS-CoV-2 human monoclonal antibody. *Proc. Natl. Acad. Sci. USA* 119, e2120976119.
42. Yamaoka, Y., Miyakawa, K., Jeremiah, S.S., Funabashi, R., Okudela, K., Kikuchi, S., Katada, J., Wada, A., Takei, T., Nishi, M., et al. (2021). Highly specific monoclonal antibodies and epitope identification against SARS-CoV-2 nucleocapsid protein for antigen detection tests. *Cell Rep. Med.* 2, 100311. <https://www.sciencedirect.com/science/article/pii/S2666379121001543>.
43. Minor, W., Cymborowski, M., Otwinowski, Z., and Chruszcz, M. (2006). HKL-3000: the integration of data reduction and structure solution—from diffraction images to an initial model in minutes. *Acta Crystallogr. D Biol. Crystallogr.* 62, 859–866. [http://www.ncbi.nlm.nih.gov/entrez/query.fcgi?cmd=Retrieve&db=PubMed&dopt=Citation&list\\_uids=16855301](http://www.ncbi.nlm.nih.gov/entrez/query.fcgi?cmd=Retrieve&db=PubMed&dopt=Citation&list_uids=16855301).
44. Winn, M.D., Ballard, C.C., Cowtan, K.D., Dodson, E.J., Emsley, P., Evans, P.R., Keegan, R.M., Krissinel, E.B., Leslie, A.G.W., McCoy, A., et al. (2011). Overview of the CCP4 suite and current developments. *Acta Crystallogr. D Biol. Crystallogr.* 67, 235–242. <https://www.ncbi.nlm.nih.gov/pubmed/21460441>.
45. Vagin, A., and Teplyaev, A. (2010). Molecular replacement with MOLREP. *Acta Crystallogr. D Biol. Crystallogr.* 66, 22–25. <http://www.ncbi.nlm.nih.gov/pubmed/20057045>.
46. Emsley, P., and Cowtan, K. (2004). Coot: model-building tools for molecular graphics. *Acta Crystallogr. D Biol. Crystallogr.* 60, 2126–2132. [http://www.ncbi.nlm.nih.gov/entrez/query.fcgi?cmd=Retrieve&db=PubMed&dopt=Citation&list\\_uids=15572765](http://www.ncbi.nlm.nih.gov/entrez/query.fcgi?cmd=Retrieve&db=PubMed&dopt=Citation&list_uids=15572765).
47. Adams, P.D., Afonine, P.V., Bunkóczi, G., Chen, V.B., Davis, I.W., Echols, N., Headd, J.J., Hung, L.W., Kapral, G.J., Grosse-Kunstleve, R.W., et al. (2010). PHENIX: a comprehensive Python-based system for macromolecular structure solution. *Acta Crystallogr. D Biol. Crystallogr.* 66, 213–221.
48. Murshudov, G.N., Skubák, P., Lebedev, A.A., Pannu, N.S., Steiner, R.A., Nicholls, R.A., Winn, M.D., Long, F., and Vagin, A.A. (2011). REFMAC5 for the refinement of macromolecular crystal structures. *Acta Crystallogr. D* 67, 355–367.
49. Schwede, T., Kopp, J., Guex, N., and Peitsch, M.C. (2003). SWISS-MODEL: an automated protein homology-modeling server. *Nucleic Acids Res.* 31, 3381–3385.
50. Jumper, J., Evans, R., Pritzel, A., Green, T., Figurnov, M., Ronneberger, O., Tunyasuvunakool, K., Bates, R., Židek, A., Potapenko, A., et al. (2021). Highly accurate protein structure prediction with AlphaFold. *Nature* 596, 583–589.
51. Bajpai, S., Petkov, B.K., Tong, M., Abreu, C.R.A., Nair, N.N., and Tuckerman, M.E. (2023). An interoperable implementation of collective-variable based enhanced sampling methods in extended phase space within the OpenMM package. *J. Comput. Chem.* 44, 2166–2183.
52. Chen, L., Cruz, A., Roe, D.R., Simmonett, A.C., Wickstrom, L., Deng, N., and Kurtzman, T. (2021). Thermodynamic Decomposition of Solvation Free Energies with Particle Mesh Ewald and Long-Range Lennard-Jones Interactions in Grid Inhomogeneous Solvation Theory. *J. Chem. Theor. Comput.* 17, 2714–2724.
53. Eschenfeldt, W.H., Makowska-Grzyska, M., Stols, L., Donnelly, M.I., Jedrzejczak, R., and Joachimiak, A. (2013). New LIC vectors for production of proteins from genes containing rare codons. *J. Struct. Funct. Genom.* 14, 135–144.
54. Makowska-Grzyska, M., Kim, Y., Maltseva, N., Li, H., Zhou, M., Joachimiak, G., Babnigg, G., and Joachimiak, A. (2014). Protein Production for Structural Genomics Using *E. coli* Expression. In *Structural Genomics and Drug Discovery: Methods and Protocols*, W.F. Anderson, ed. (Springer New York), pp. 89–105.
55. Kim, Y., Jedrzejczak, R., Maltseva, N.I., Wilamowski, M., Endres, M., Godzik, A., Michalska, K., and Joachimiak, A. (2020). Crystal structure of Nsp15 endoribonuclease NendoU from SARS-CoV-2. *Protein Sci.* 29, 1596–1605.
56. Guthmiller, J.J., Dugan, H.L., Neu, K.E., Lan, L.Y., and Wilson, P.C. (2019). An Efficient Method to Generate Monoclonal Antibodies from Human B Cells. In *Human Monoclonal Antibodies: Methods and Protocols*, M. Steinitz, ed. (Springer New York), pp. 109–145.
57. Kim, Y., Babnigg, G., Jedrzejczak, R., Eschenfeldt, W.H., Li, H., Maltseva, N., Hatzos-Skintges, C., Gu, M., Makowska-Grzyska, M., Wu, R., et al. (2011). High-throughput protein purification and quality assessment for crystallization. *Methods* 55, 12–28. <http://www.sciencedirect.com/science/article/pii/S1046202311001605>.
58. Rosenbaum, G., Alkire, R.W., Evans, G., Rotella, F.J., Lazarski, K., Zhang, R.G., Ginell, S.L., Duke, N., Naday, I., Lazarz, J., et al. (2006). The Structural Biology Center 19ID undulator beamline: facility specifications and protein crystallographic results. *J. Synchrotron Radiat.* 13, 30–45. <http://www.ncbi.nlm.nih.gov/pmc/articles/PMC2603069/>.
59. French, S., and Wilson, K. (1978). On the treatment of negative intensity observations. *Acta Crystallogr., Sect. A* 34, 517–525.

60. Padilla, J.E., and Yeates, T.O. (2003). A statistic for local intensity differences: robustness to anisotropy and pseudo-centering and utility for detecting twinning. *Acta Crystallogr. D* 59, 1124–1130.
61. Murshudov, G.N., Vagin, A.A., and Dodson, E.J. (1997). Refinement of Macromolecular Structures by the Maximum-Likelihood Method. *Acta Crystallogr. D* 53, 240–255.
62. Davis, I.W., Leaver-Fay, A., Chen, V.B., Block, J.N., Kapral, G.J., Wang, X., Murray, L.W., Arendall, W.B., 3rd, Snoeyink, J., Richardson, J.S., and Richardson, D.C. (2007). MolProbity: all-atom contacts and structure validation for proteins and nucleic acids. *Nucleic Acids Res.* 35, W375–W383.
63. Laskowski, R.A., MacArthur, M.W., Moss, D.S., and Thornton, J.M. (1993). PROCHECK: a program to check the stereochemical quality of protein structures. *J. Appl. Crystallogr.* 26, 283–291.
64. Bjelkmar, P., Larsson, P., Cuendet, M.A., Hess, B., and Lindahl, E. (2010). Implementation of the CHARMM Force Field in GROMACS: Analysis of Protein Stability Effects from Correction Maps, Virtual Interaction Sites, and Water Models. *J. Chem. Theor. Comput.* 6, 459–466.
65. Ramanathan, A., and Agarwal, P.K. (2009). Computational Identification of Slow Conformational Fluctuations in Proteins. *J. Phys. Chem. B* 113, 16669–16680.

## STAR★METHODS

### KEY RESOURCES TABLE

REAGENT or RESOURCE	SOURCE	IDENTIFIER
<b>Antibodies</b>		
S24-1063	This work	N/A
S24-1564	This work	N/A
S24-1636	This work	N/A
S24-178	This work	N/A
S24-188	This work	N/A
S24-202	This work	N/A
<b>Bacterial and virus strains</b>		
<i>E. coli</i> BL21(De3)-Gold	Sigma-Aldrich	69450-M
CD3-/CD19+/Antigen-PE/APC+	Thermo Fisher	22-1903-72
293T cells	Thermo Fisher	K1687
<b>Biological samples</b>		
Expression plasmid pMCSG53	N/A	N/A
<b>Chemicals, peptides, and recombinant proteins</b>		
Tobacco Etch Mosaic Virus protease	Expressed and produced in the lab	Ref. 44
LB Lennox medium	Research Products International	L24045–5000.0
Ni <sup>2+</sup> Sepharose	Cytiva	17526802
Flex-Column	Capital Scientific	KIM-420401-2510
Superdex S200 16/600 column	Cytiva	28989335
Protein A agarose beads	Thermo Fisher	20334
MCSG1-4 crystallization screens	Anatrace	50-109-1424/50-109-1514/ 50-109-1705/50-109-1609
SaltRX, INDEX	Hampton	HR2-136/HR2-134
PACT	JBS Jena BioScience	CS-207L
Proplex HT-96	Molecular Dimensions	MD1-Y2
<b>Critical commercial assays</b>		
B cell EasySep™ enrichment kit	STEMCELL	19054
<b>PDB Deposited data</b>		
NPRBD coordinates	This work	PDB 6vyo
NPRBD coordinates	This work	PDB 6wkp
NPRBD/S24-1379 coordinates	This work	PDB 7sts
NPRBD/S24-188 coordinates	This work	PDB 7sue
NPRBD/S24-1063 coordinates	This work	PDB 7str
NPRBD/S24-1564 coordinates	This work	PDB 7n3c
NPRBD/S24-202 coordinates	This work	PDB 7n3d
Human subjects	No human cohorts were used for these studies, only discarded blood cell byproducts from plasma donations by anonymous donor to the University of Chicago blood bank.	N/A

(Continued on next page)

**Continued**

REAGENT or RESOURCE	SOURCE	IDENTIFIER
<b>Recombinant DNA</b>		
NP <sup>RBD</sup> synthetic gene UniProtKB – P0DTC9 res. 48-173	Twist Biosciences	N/A
Fab synthetic genes	Integrated DNA Technologies	N/A
<b>Software and algorithms</b>		
HKL3000 suite	W. Minor, M. Cymborowski, Z. Otwinowski and M. Chruszcz <sup>43</sup>	<a href="https://hkl-xray.com/hkl-3000">https://hkl-xray.com/hkl-3000</a>
CCP4 package	Collaborative Computational Project <sup>44</sup>	<a href="https://www.ccp4.ac.uk">https://www.ccp4.ac.uk</a>
Molrep software	A. Vagin and A. Teplyakov <sup>45</sup>	molrep-automated program for molecular replacement
Coot	P. Emsley and K. Cowtan <sup>46</sup>	<a href="https://www2.mrc-lmb.cam.ac.uk/personal/pemsley/coot/">https://www2.mrc-lmb.cam.ac.uk/personal/pemsley/coot/</a>
Phenix	Cambridge University; Duke University; Lawrence Berkeley National Laboratory; Los Alamos National Laboratory <sup>47</sup>	<a href="https://www.phenix-online.org/">https://www.phenix-online.org/</a>
Refmac	G. N. Murshudov, P. Skubak, A. A. Lebedev, N. S. Pannu, R. A. Steiner, R. A. Nicholls et al. <sup>48</sup>	Refmac version 5.0.32 - macromolecular refinement program
SWISS-MODEL	Schwede, T. et al. <sup>49</sup>	<a href="https://swissmodel.expasy.org">https://swissmodel.expasy.org</a>
AlphaFold2	Jumper, J. et al. <sup>50</sup>	<a href="https://www.deepmind.com/open-source/alphafold">https://www.deepmind.com/open-source/alphafold</a>
OpenMM software package	Bajpai, S. et al. <sup>51</sup>	<a href="https://openmm.org">https://openmm.org</a>
Particle Mesh Ewald method	Chen, L. et al. <sup>52</sup>	<a href="https://doi.org/10.1021/acs.jctc.0c01185">https://doi.org/10.1021/acs.jctc.0c01185</a>

**RESOURCE AVAILABILITY****Lead contact**

Further information and requests for reagents should be addressed to the lead contact, Dr. Andrzej Joachimiak ([andrzej@anl.gov](mailto:andrzej@anl.gov)).

**Materials availability**

Synthetic genes for the following Fabs were generated by *Integrated DNA Technologies*: S24–1063, S24–1564, S24–1636, S24–178, S24–188 and S24-202 and for NP<sup>RBD</sup> synthetic gene UniProtKB – P0DTC9 res. 48–173 by *Twist Biosciences*.

**Data and code availability**

Data: further information and requests for resources and reagents should be directed to and will be fulfilled by the **lead contact**, Andrzej Joachimiak, Structural Biology Center, X-ray Science Division, Argonne National Laboratory, Lemont, Illinois 60439, USA, Phone: 630-252-3926; fax: 630-252-6126; e-mail: [andrzej@anl.gov](mailto:andrzej@anl.gov).

Code: the atomic coordinates, structure factors and protein sequences have been deposited in the PDB under accession codes 6vyo (<https://doi.org/10.2210/pdb6VYO/pdb>), and 6wkp (<https://doi.org/10.2210/pdb6WKP/pdb>) for NP<sup>RBD</sup> and 7str (<https://doi.org/10.2210/pdb7STR/pdb>), 7n3c (<https://doi.org/10.2210/pdb7N3C/pdb>), 7sts (<https://doi.org/10.2210/pdb7STS/pdb>), 7sue (<https://doi.org/10.2210/pdb7SUE/pdb>), and 7n3d (<https://doi.org/10.2210/pdb7N3D/pdb>) for NP<sup>RBD</sup>/S24-1063, NP<sup>RBD</sup>/S24-1564, NP<sup>RBD</sup>/S24-1379, NP<sup>RBD</sup>/S24-188, and NP<sup>RBD</sup>/S24-202, respectively. These data are freely available to scientific community.

**Human samples**

No human cohorts were used for these studies, only discarded blood cell byproducts from plasma donations by anonymous convalescent patient infected by SARS-CoV-2 donating to the University of Chicago blood bank. Several mAbs were isolated using an antigen-bait sorting and single-cell sequencing approach. The sequences of Fabs are available in the PDB under accession codes 7str, 7n3c, 7sts, 7sue, and 7n3d for NP<sup>RBD</sup>/S24-1063, NP<sup>RBD</sup>/S24-1564, NP<sup>RBD</sup>/S24-1379, NP<sup>RBD</sup>/S24-188, and NP<sup>RBD</sup>/S24-202, respectively.

**EXPERIMENTAL MODEL AND STUDY PARTICIPANT DETAILS**

No applicable to this study.

## METHOD DETAILS

### Gene cloning, protein expression and purification of NP<sup>RBD</sup>

Gene fragment coding of nucleocapsid protein from SARS-CoV-2 was codon-optimized for efficient expression in *E. coli*. The coding sequence of NP<sup>RBD</sup> comprising residues Asn48 to Ala173 (UniProtKB – P0DTC9) was synthesized and cloned into pMCSG53 by Twist Biosciences, USA. Cloning into pMCSG53 vector introduced a His<sub>6</sub>-tag at the N-terminus of NP<sup>RBD</sup>, followed by a cleavage site for Tobacco Etch Mosaic Virus (TEV) protease.<sup>53</sup> For NP<sup>RBD</sup> expression, the plasmid was transformed into *E. coli* BL21(DE3)-Gold cells (Stratagene) using heat-shock.<sup>54</sup> After the transformation, bacterial cells were precultured overnight at 37°C in 100 mL of LB Lennox medium supplemented with 40 mM K<sub>2</sub>HPO<sub>4</sub> and 160 mg/L of ampicillin. Subsequently, 40 mL of overnight cultures was used to inoculate 4 L of LB with 40 mM K<sub>2</sub>HPO<sub>4</sub> and 160 mg/L ampicillin. Next, the cells were incubated at 37°C with 180 RPM shaking for approximately 3 h until reaching optical density at 600 nm equal to 1. Subsequently, the bacterial culture was cooled down for 1 h in an incubator set to 4°C with 180 RPM shaking. Expression of NP<sup>RBD</sup> was induced with 0.2 mM isopropyl β-D-1-thiogalactopyranoside, supplemented with 0.1% glucose, and incubated overnight at 16°C. Bacterial cells were harvested by centrifugation at 4°C, 5000 RCF for 10 min. Cell pellets were resuspended in lysis buffer 50 mM HEPES pH 8.0, 500 mM NaCl, 5% v/v glycerol, 20 mM imidazole, and 10 mM β-mercaptoethanol (1 g of cells: 5 mL of lysis buffer) for purification or frozen and stored at –80°C until purification.

Bacterial cells were lysed by sonication on ice using 120 W output power for 5 min (4 s pulses of sonication followed by 20 s breaks). After sonication, samples were centrifuged to remove cellular debris (30k RCF, 4°C, 1 h). We used a vacuum-assisted purification system to perform NP<sup>RBD</sup> purification with immobilized metal affinity chromatography (IMAC).<sup>55</sup> Using 5 mL of Ni<sup>2+</sup> Sepharose (Cytiva) loaded on a Flex-Column (420400–2510 Kontes, Capital Scientific) attached to a Vac-Man vacuum system (Promega), beads were equilibrated in a lysis buffer. The cell lysate was loaded on the column, and Ni<sup>2+</sup> Sepharose was washed using 20 column volumes of lysis buffer. For elution, the lysis buffer was supplemented with imidazole up to 500 mM (pH 8). To remove His<sub>6</sub>-Tag after elution, we used TEV protease added in a molar ratio 1 TEV to 40 NP<sup>RBD</sup> and incubated for 24 h at 22°C. The protein was purified using second IMAC chromatography with flow through collected. TEV cleavage leaves three residues SNA at the N-terminus of NP<sup>RBD</sup>. Next, NP<sup>RBD</sup> was concentrated using 10 kDa cutoff centrifugal protein concentrators (Merck-Millipore). Subsequently, we performed SEC of NP<sup>RBD</sup> using a Superdex S200 16/600 column attached to an ÅKTA xpress (Cytiva) purification system. Size exclusion chromatography was done at 4°C in a buffer containing 20 mM HEPES, 500 mM NaCl, 5% (v/v) glycerol, 10 mM β-mercaptoethanol, pH 8.0. Purified fractions of NP<sup>RBD</sup> from the middle of the SEC elution peak were concentrated to final concentration of 50.0 mg/mL. Protein was flash cooled using 40 μL aliquots dropped directly into liquid nitrogen. Samples were stored at –80°C. Upon thawing, the samples were used for crystallization experiments.

### Preparation of mAbs/NP<sup>RBD</sup> complexes for crystallization

Fabs or mAbs (S24–1063, S24–1564, S24–1636, S24–178, S24–188, and S24–202 in concentration of 1.9–7.3 mg/mL) were obtained from B-cells of COVID-19 convalescent patient.<sup>28</sup> The mAbs were generated as previously described.<sup>28</sup> Peripheral blood mononuclear cell (PBMCs) was isolated from a subject upon recovery from SARS-CoV-2 viral infection and subsequently enriched for B cells using the human pan B cell EasySep enrichment kit (STEMCELL). The COVID-19 antigen probes (NP<sup>RBD</sup>, Spike<sup>RBD</sup> and ORF8) were generated by conjugating distinct PE or APC-streptavidin (SA)-oligos (Biolegend) to each biotinylated antigen. The cells that were viable/CD3-/CD19+/Antigen-PE/APC+ were sorted as probe positive B cells and immediately process for the generation of 10X Genomic libraries. Via linking BCR to antigen specificity through sequencing (LIBRA-seq), B cells that specifically bound to SARS-CoV-2 NP<sup>RBD</sup> probe with high intensity were chosen for further analysis. Immunoglobulin heavy and light chain genes obtained from VDJ sequencing analysis of NP<sup>RBD</sup>-specific clones were synthesized by Integrated DNA Technologies. Cloning, transfection, and mAb purification have been previously described.<sup>56</sup> Briefly, sequences of NP<sup>RBD</sup> probe-specific B cells were cloned into human IgG1 expression vectors using Gibson assembly, and heavy and light genes were co-transfected into 293T cells (Thermo Fisher). Secreted mAbs were purified from the supernatant using protein A agarose beads (Thermo Fisher). The Fabs were mixed with NP<sup>RBD</sup> at ratio 1:1.2 and were incubated for 30 min.

### Crystallization experiments

Crystallization screens were performed by the sitting-drop vapor-diffusion method in 96-well CrystalQuick plates (Greiner Bio-One).<sup>57</sup> The plates were set up using Mosquito liquid dispenser (TTP LabTech) utilizing 400 nL of NP<sup>RBD</sup> and the complexes with mAb fragments were mixed with 400 nL of well solution and equilibrated against 135 nL reservoir solution. In all cases, the plates were incubated at 289 K. The crystallization screening was performed using MCSG1 and MCSG4 (Anatrace), SaltRX (Hampton), PACT (Qiagen), Proplex HT-96 (Molecular Dimensions) and INDEX (Hampton) screens. For NP<sup>RBD</sup> two crystal forms were obtained after three days: the orthorhombic crystals from the condition containing 0.1 M MES, 10 mM zinc chloride and 20% PEG6000 at pH 6.0 and the monoclinic crystals grown at pH 6.5 using 0.1 M MES and 30% PEG4000. Crystals of the complexes of NP<sup>RBD</sup> and mAb fragments appeared after 2–3 days: the crystals of NP<sup>RBD</sup>/S24-1063 are from the condition containing 0.1 M Bis-Tris pH 5.5 and 25% (w/v) PEG 3350, NP<sup>RBD</sup>/S24-1564 from 0.2 M magnesium chloride hexahydrate, 0.1 M HEPES pH 7.5 and 25% (w/v) PEG 3350, NP<sup>RBD</sup>/S24-1379 from 0.2 M calcium chloride, 0.1 M Tris pH 8.0 and 20% (w/v) PEG 6000, NP<sup>RBD</sup>/S24-188 from 0.1 M sodium citrate pH 5.6, 20% (w/v) PEG 4000, and 20% (v/v) 2-propanol, and NP<sup>RBD</sup>/S24-202 from 0.2 M potassium iodide and 20% (w/v) PEG 3350.

### Data collection, structure determination and refinement

Prior to flash-cooling in liquid nitrogen, the crystals were cryoprotected in their mother liquor supplemented with up to 25% of glycerol or ethylene glycol. The X-ray diffraction experiments were carried out at 100 K, at the Structural Biology Center 19-ID beamline at the Advanced Photon Source, Argonne National Laboratory.<sup>58</sup> The diffraction images were recorded on the PILATUS3 X 6M detector. The dataset was processed and scaled with the HKL3000 suite.<sup>43</sup> Intensities were converted to structure factor amplitudes in the Truncate program<sup>59,60</sup> from the CCP4 package.<sup>44</sup> The NP<sup>RBD</sup> structure was determined by molecular replacement (MR) using Molrep<sup>45</sup> implemented in the HKL3000 software package and SARS-CoV-1 NP<sup>RBD</sup> structure (PDB id: 2ajf) as a search model. The monoclinic structure was solved by MR with a refined SARS-CoV-2 NP<sup>RBD</sup> as a model. In both cases, the initial solution was manually adjusted using Coot<sup>46</sup> and then iteratively refined using Coot, Phenix<sup>47</sup> and Refmac.<sup>48,61</sup> The structures of the complexes of NP<sup>RBD</sup> and mAb fragments were determined by an analogous protocol MR, with the search models for the mAb fragments generated with SWISS-MODEL<sup>49</sup> and the structure of NP<sup>RBD</sup> (PDB id: 6vyo) used as a probe for the N protein search. In all NP<sup>RBD</sup>/Fab complexes, the initial solutions required significant manual adjustments, particularly for mAb fragments, due to severe conformational discrepancies between the search models and the electron density calculated from the solutions. The following iterative refinement using Coot and Phenix were carried out till the structures converged to reasonable  $R_w/R_{free}$  with good stereochemistry. All structures, except for NP<sup>RBD</sup>/S24-1063 (1.50 Å) and NP<sup>RBD</sup>/S24-1564 (1.53 Å), were refined with TLS parameterization of anisotropic displacement parameters (ADP) and for the structures of NP<sup>RBD</sup>/S24-1063 and NP<sup>RBD</sup>/S24-1564 full ADP refinements were calculated. Throughout the refinement, the same 5% of reflections were kept out throughout from the refinement (in both Refmac and Phenix refinements). The final models show nearly complete polypeptide chains. The residues that have not been modeled due to the lack of interpretable electron density for each of the structures are listed in [Tables S1](#) and [S2](#). The stereochemistry of the structure was checked with MolProbity<sup>62</sup> and PROCHECK<sup>63</sup> and validated with the PDB validation server. The data collection and processing statistics are given in [Table S1](#). Data reported in this paper will be shared by the lead contact upon request. The atomic coordinates, structure factors and protein sequences have been deposited in the PDB under accession codes 6vyo, and 6wkp for NP<sup>RBD</sup> and 7str, 7n3c, 7sts, 7sue, and 7n3d for NP<sup>RBD</sup>/S24-1063, NP<sup>RBD</sup>/S24-1564, NP<sup>RBD</sup>/S24-1379, NP<sup>RBD</sup>/S24-188, and NP<sup>RBD</sup>/S24-202, respectively. This paper does not report original code. Any additional information required to re-analyze the data reported in this paper is available from the [lead contact](#) upon request.

### AlphaFold and molecular dynamics simulations

The full sequence of SARS-CoV-2 NP was modeled with AlphaFold2 multimer models.<sup>50</sup> The input fasta file consisted of two identical chains. The prediction was performed on Nvidia V100 GPUs and it generated 5 structures from 5 independent AlphaFold models. The structures were ranked by model confidence score.

MD simulation can provide valuable insights of protein dynamics in atomistic scale. To understand the binding between NP<sup>RBD</sup> and mAbs, we simulated the 3 structures of NP<sup>RBD</sup>/S24 complexes (202, 1063, 1379) with the most complete RBD structures. NP<sup>RBD</sup>/S24-202 and NP<sup>RBD</sup>/S24-1063 consist of a single mAbs with a heavy chain and a light chain, and NP<sup>RBD</sup>. NP<sup>RBD</sup>/S24-1379 is a dimer with two sets of antibody/antigen pairs. The MD simulations were carried out via OpenMM software package on CUDA platform with mixed precision.<sup>51</sup> The molecular topologies were parameterized with the charmm27 force field.<sup>64</sup> Each system was solvated in a  $15^3$  nm<sup>3</sup> box with tip3p water model and minimized/equilibrated as outlined in previous studies.<sup>65</sup> The simulations were run with 2 fs timestep that was integrated using Langevin integrator at 310 K with  $1 \text{ ps}^{-1}$  heat bath friction coefficient. The pressure was maintained at 1 bar with Monte Carlo Barostat. The nonbonded interactions were cutoff at 1 nm, and the long-range coulombic force was calculated with Particle Mesh Ewald method.<sup>52</sup> The simulation wrote to the trajectory every 50 ps for 200 ns and 3 replicas. We then assessed the chain stability with Root-Mean-Square Fluctuation. We also run MD simulation on the full-length NP structure from the AlphaFold to understand the binding antibody impact to the NP<sup>RBD</sup> dynamics.